

## Design of Nonlinear Uncertainty Controller for Grid-Tied Solar Photovoltaic System Using Sliding Mode Control

D. Menaga<sup>1</sup>, M. Premkumar<sup>2</sup>, R. Sowmya<sup>1,\*</sup> and S. Narasimman<sup>3</sup>

<sup>1</sup>National Institute of Technology, Tiruchirappalli, 620015, India

<sup>2</sup>GMR Institute of Technology, Rajam, 532127, India

<sup>3</sup>Adhiparasakthi College of Engineering, Vellore, 632506, India

\*Corresponding Author: R. Sowmya. Email: sowmyanitt@gmail.com

Received: 31 July 2020; Accepted: 09 August 2020

**Abstract:** The proposed controller accompanies with different sliding surfaces. To understand maximum power point extraction as opposed to nonlinear uncertainties and unknown disturbance of a grid-connected photovoltaic system to various control inputs ( $u_d, u_q$ ) is designed. To extract maximum power from a solar array and maintain unity power flow in a grid by controlling the voltage across the dc-link capacitor ( $V_{pvdc}$ ) and reactive current ( $i_q$ ). A multiple input-output with multiple uncertainty constraints have considered designing proposed sliding mode controllers to validated their robustness performance. An innovative controller verifies uncertain inputs, constant and changes in irradiances, and temperature of the photo-voltaic system. These controllers do not limit the parametric uncertainties and disturbances on the system, which shows the significance of the developed designs. The performance characteristics have been compared to two sliding mode controllers and validated through numerical simulation for both normal and robustness conditions.

**Keywords:** Grid-connected; multiple input-output systems; nonlinear control design; photovoltaic system; sliding mode control; uncertainty

### Nomenclature

MPPT:	Maximum Power Point Tracking
$l$ :	Filter Inductor
$r$ :	Resistance
$V_{pvdc}$ :	Solar Array Voltage
$I_{pv}$ :	Solar Array Current
$v_{dc}$ :	Voltage Across the DC-Link Capacitor
$V_{pvdc\text{ref}}$ :	Voltage Reference from MPPT
$I_{d\text{ref}}$ :	Current Reference from MPPT
$I_a, I_b, I_c$ :	Grid Current
$V_a, V_b, V_c$ :	Inverter Output Voltages
$E_a, E_b, E_c$ :	Grid Voltages
$E_d, E_q$ :	D-Q Axis Grid Voltages



This work is licensed under a Creative Commons Attribution 4.0 International License, which permits unrestricted use, distribution, and reproduction in any medium, provided the original work is properly cited.

$I_d, I_q$ :	D-Q Axis Grid Current
$\omega$ :	Grid Angular Frequency
$S_1, S_2$ :	Sliding Surfaces
$u_1, u_2$ :	Control Law
$P_{PV}$ :	PV Power

## 1 Introduction

In recent days, renewable energy utilization has become popular due to increased demand for electricity and the availability of advanced conversion technologies. The photovoltaic power conversion is a popular method, as solar energy is directly converted to electrical units. Solar energy is free from pollution, inexhaustible, and distributed continuously to earth. The ability and effective performance of the PV (photo-voltaic) power plants are validated under different operating conditions with respect to the constant power algorithm [1]. Several PV tracking aspects and mechanisms are discussed with various technologies based on their characteristic performances [2]. Many grid-connected photovoltaic control topologies are discussed with their challenges, requirements, and IEEE standards [3]. The desired steady-state and dynamic behavior of the synchronized system is evaluated by different technologies in grid-connected PV plants [4]. The control approaches of a single-stage PV system are discussed with their maximum power tracking, voltage, and power control in grid synchronization networks [5]. Power loss performance is investigated with a single stage and double stage power conversion system. A single-stage power conversion system overcomes the double stage conversion system due to good power quality, low cost, high efficiency, and reduced maintenance [6,7]. Extracted maximum power is delivered to the grid from a solar plant by maintaining unity power flow control in the grid using different nonlinear designs in the photovoltaic system [8–17]. Also, for unbalanced grid voltage systems [9,10] and uncertainties in the systems [10,12,18]. In the literature survey [10,13,14,18], a sliding mode controller is a robust nonlinear control to extract maximum solar power and assured unity power flow control in the grid-connected PV system against parametric, uncertainties variations are explained with different control laws. Several power point tracking technologies [15,19–22], are implemented with various algorithms in the photovoltaic system.

The sliding mode controller (SMC) is a robust nonlinear control technique that controls nonlinear uncertainties and unknown disturbances in the model. The dynamic behavior of the proposed system is concerned with the control law of the sliding surfaces. This photovoltaic grid-connected system is examined for standard and changing atmospheric conditions. Disturbances in the grid-connected photovoltaic system may occur due to solar irradiance, temperature variations, atmospheric changes, and climate variation. The main target of the proposed system is to track maximum power from a solar array by regulating the dc-link voltage across the capacitance of the inverter model. To make unit power factor in the grid to ensure q-axis current as zero using different sliding surfaces. The trajectories have been forcing to reach the sliding manifold in finite-time to achieve the control objectives. Proposed controller surfaces are designed with all uncertainty changes in the system, and it is assumed to be bounded conditions within the known bounds. A proposed controller's effectiveness has been validating through numerical simulations for both normal and robustness condition.

The rest of the paper is organized as follows: The proposed photovoltaic system's mathematical modeling and problem formulation are given in Sections 2, while the controller design is explained in Section 3. The controller's simulation result and discussion, and its comparison are presented in Section 4, followed by the conclusion in Section 5.

## 2 Mathematical Modelling and Problem Formulation

### 2.1 Mathematical Modelling

A three-phase grid-connected photovoltaic system model is shown in Fig. 1. This system's inverter output power is provided to the grid supply through a filter inductance ( $l$ ) and connecting lines ( $r$ ) in a single stage with the help of a dc-link capacitor. A three-phase grid voltage and current are represented through the phases A, B, C, in-terms of  $E_a, E_b, E_c$  and  $I_a, I_b, I_c$ . This three-phase ac voltage and current dynamics are changed into dc values  $E_d, E_q$  and  $I_d, I_q$  through  $d, q$  reference rotating transformation model by,

$$\begin{aligned} l \frac{dx_1}{dt} &= -rx_1 + \omega x_2 - E_d + u_d \\ l \frac{dx_2}{dt} &= -rx_2 - \omega x_1 - E_q + u_q \end{aligned} \quad (1)$$

The following equation expresses a power balance between the dc photovoltaic input and AC grid output,

$$\begin{aligned} E_d x_1 + E_q x_2 &= v_{pvdc} i_{dc}; \quad C \dot{v}_{pvdc} = i_{pv} - i_{dc} \\ \dot{v}_{pvdc} &= \frac{1}{C} \left[ i_{pv} - \left( \frac{E_d x_1 + E_q x_2}{x_3} \right) \right] \end{aligned} \quad (2)$$

Let us consider as  $x_1 = I_d$ ,  $x_2 = I_q$ ,  $x_3 = v_{pvdc}$ . Photo-voltaic, dc-link current can be measured in terms of  $i_{pv}$ ,  $i_{dc}$ . Where the system variables  $E_d, E_q$  and  $I_d, I_q$  are the grid  $d, q$  axis voltages and currents,  $u_d, u_q$  are the  $d, q$  axis output voltages of the inverter, grid frequency ( $\omega$ ), respectively. The system Eqs. (1) and (2) can be modified with dynamic uncertainty changes by the following equations.

$$\begin{aligned} \dot{x}_1 &= -\frac{r}{l} x_1 + \omega x_2 - \frac{E_d}{l} + \frac{u_d}{l} + \frac{\xi_d}{l} \\ \dot{x}_2 &= -\frac{r}{l} x_2 - \omega x_1 - \frac{E_q}{l} + \frac{u_q}{l} + \frac{\xi_q}{l} \\ \dot{x}_3 &= \left[ \frac{\xi_{x_3}}{C} - \frac{E_d x_1 + E_q x_2}{C x_3} \right] \end{aligned} \quad (3)$$

The system uncertainties  $\xi_d$ ,  $\xi_q$  and  $\xi_{v_{dcpv}}$  can be represented by the following equations,

$$\begin{aligned} \xi_d &= \Delta r x_1 - \omega \Delta l x_2 + \Delta E_d + \Delta l \dot{x}_1 + \phi_d \\ \xi_q &= -\Delta r x_2 + \omega \Delta l x_1 + \Delta E_q + \Delta l \dot{x}_2 + \phi_q \\ \xi_{v_{dcpv}} &= \frac{1}{x_3} (E_d \Delta x_1 + \Delta E_d (x_1 + \Delta x_1) + E_q \Delta x_2 + \Delta E_q (x_2 + \Delta x_2)) \\ &\quad + \Delta C \dot{x}_3 + \Delta v + i_{pv} + \phi_v \end{aligned} \quad (4)$$

where  $dq$  axis uncertainty currents ( $\Delta x_1, \Delta x_2$ ), grid uncertainty voltages ( $\Delta E_d, \Delta E_q$ ), and other external system disturbances ( $\phi_d, \phi_q, \phi_v$ ) like dynamic response changes in the nonlinear module and angular frequency are caused due to variations in the system parametric ( $\Delta r, \Delta l$ ), uncertainty voltage changes in the dc-link can be measured in terms of ( $\Delta v$ ). All uncertainty changes in the system are assumed to be bounded conditions within the known bounds.

In the proposed system, the photovoltaic current ( $i_{pv}$ ) and power changes take into the account-of system dynamics by slowly making small parameter variations in the module parameters. Time derivatives of all three uncertainty ( $\xi_d, \xi_q, \xi_v$ ) variables are considered to be bounded with around zero condition as time  $t \rightarrow \infty$ . The derivatives of uncertainty dynamics ( $\dot{\xi}_d, \dot{\xi}_q, \dot{\xi}_{v_{dcpv}}$ ) are assumed to be zero for stability control  $\dot{\xi}_d = 0, \dot{\xi}_q = 0, \dot{\xi}_{v_{dcpv}} = 0$ .

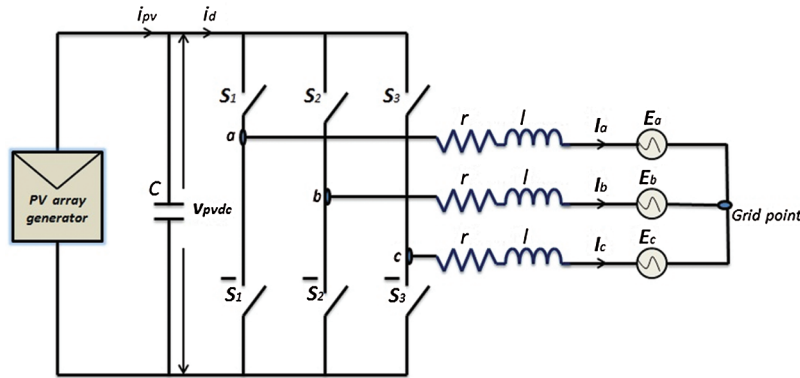


**Figure 1:** Three-phase grid-connected photovoltaic system

The proposed PV system state model can be expressed from the Eq. (3) with control inputs ( $u_d, u_q$ ) and control outputs ( $x_2, x_3$ ), multiple input, multiple output, uncertainty nonlinear, and the mathematical state model is given by

$$\dot{x} = f(x) + g_1(x)u + g_2(x)\xi$$

$$\dot{x} = \begin{pmatrix} -\left(\frac{r}{l}\right)x_1 + \omega x_2 - \frac{E_d}{l} \\ -\left(\frac{r}{l}\right)x_2 + \omega x_1 - \frac{E_q}{l} \\ -\left(\frac{E_d x_1 + E_q x_2}{C x_3}\right) \end{pmatrix} + \begin{pmatrix} \frac{1}{l} & 0 \\ 0 & \frac{1}{l} \\ 0 & 0 \end{pmatrix} \begin{pmatrix} u_d \\ u_q \end{pmatrix} + \begin{pmatrix} \frac{1}{l} & 0 & 0 \\ 0 & \frac{1}{l} & 0 \\ 0 & 0 & \frac{1}{C} \end{pmatrix} \begin{pmatrix} \xi_d \\ \xi_q \\ \xi_{v_{dcpv}} \end{pmatrix} \quad (5)$$

The output vector,

$$y = [y_1 \ y_2]; y = [i_q \ v_{dc}] \quad (6)$$

State and disturbance vector is defined as,

$$x = [i_d \ i_q \ v_{dc}]^T = [x_1 \ x_2 \ x_3]^T; \xi = [\xi_d \ \xi_q \ \xi_{v_{dcpv}}] \quad (7)$$

### 2.2 Problem Formulation

The main objective of the 3 $\phi$  grid-connected photovoltaic system is to deliver maximum power from the solar system to the grid with unit power factor while ensuring a maximum power point tracking operation. Real power (P) and reactive power (Q) are controlled by the d and q-axis current controller components. To maintain unity power factor in the grid, their q-axis current component is set to zero, i.e.,  $i_q = 0$ . Active power flowing to the grid is controlled by keeping grid voltages in-phase with inverter current. These control objectives are achieved by tracking a pre-computed value of  $v_{pvdc}$  using an MPPT algorithm and by setting  $i_q = 0$ . Hence the control problem is defined as regulating the state  $x_2 = 0$  and track  $x_1$  to  $x_1^*$  &  $x_3$  to  $x_{3ref}$ .

### 3 Controller Designs

The main objective of the nonlinear uncertainty control designs for the grid-connected photovoltaic system is to deliver maximum power from the solar system to the grid with a unity power factor and also ensure maximum power point tracking operation by keeping sliding manifold  $M \cong S_1 = S_2 = 0$ . For designing controller inputs ( $u_d, u_q$ ), the sliding surfaces ( $S_1, S_2$ ) are set to zero. Thus, the control trajectories starting from anywhere reaching the sliding manifold M is finite-time.

### 3.1 Controller I

**Lemma 3.1.** Single-stage three-phase, grid-connected PV system, represented in the Eqs. (1) and (2) ensures unity power factor and maximum power extraction on the sliding manifold  $M \cong S_1 = S_2 = 0$ .

$$\begin{aligned} S_1 &= x_1 - x_1^* \\ S_2 &= x_2 \end{aligned} \tag{8}$$

**Proof:** On the manifold  $M = 0$ , i.e.,  $S_1 = S_2 = 0$

$$\begin{aligned} S_1 &= 0 \\ x_1 - x_1^* &= 0 \\ x_1 &\rightarrow x_1^* \text{ as } t \rightarrow \infty \end{aligned} \tag{9}$$

Since the sliding surface  $S_1$  is settled at zero, it can track the maximum power point quickly. In addition,  $S_2 = 0$  which implies that  $x_2 = 0$  assures unity power factor.

**Proposition 3.1.** The sliding manifold  $M$  is finite-time reachable using the following control law.

$$\begin{aligned} u_d &= -l\alpha_1 \text{sgn}(S_1) + \frac{r}{l}x_1 - \omega lx_2 + E_d \\ u_q &= -l\alpha_2 \text{sgn}(S_2) + \frac{r}{l}x_2 + \omega lx_1 + E_q \\ \eta_{d1} &= -\frac{\xi_d}{l} + \dot{x}_1^*; \quad \eta_q = \frac{\xi_q}{l} \\ \xi_d &= \Delta rx_1 - \omega \Delta lx_2 + \Delta E_d + \Delta l\dot{x}_1 + \phi_d \\ \xi_q &= \Delta rx_2 + \omega \Delta lx_1 + \Delta E_q + \Delta l\dot{x}_2 + \phi_q \end{aligned} \tag{10}$$

where  $\alpha_1 > |\dot{\delta}_d|$ ,  $\alpha_2 > |\dot{\delta}_q|$

**Proof:** The dynamics of  $S_1$  become,

$$\begin{aligned} \dot{S}_1 &= \dot{x}_1 - \dot{x}_1^* \\ &= -\frac{r}{l}x_1 + \omega x_2 - \frac{E_d}{l} + \frac{1}{l}(\Delta rx_1 - \omega \Delta lx_2 + \Delta E_d + \Delta lx_1 + \phi_d) + \frac{u_d}{l} - \dot{x}_1^* \\ &= -\frac{r}{l}x_1 + \omega x_2 - \frac{E_d}{l} + \frac{1}{l}(\Delta rx_1 - \omega \Delta lx_2 + \Delta E_d + \Delta l\dot{x}_1 + \phi_d) \\ &\quad + \frac{1}{l}[-l\alpha_1 \text{sgn}(S_1) + rx_1 - \omega lx_2 + E_d] - \dot{x}_1^* \\ &= -\frac{r}{l}x_1 + \omega x_2 - \frac{E_d}{l} + \frac{\Delta lx_1}{l} + \frac{\Delta rx_1}{l} - \frac{\omega \Delta lx_1}{l} + \frac{\Delta E_d}{l} + \frac{\phi_d}{l} - \alpha_1 \text{sgn}(S_1) \\ &\quad + \frac{r}{l}x_1 - \omega x_2 + \frac{E_d}{L} + \frac{\xi_d}{l} - \dot{x}_1^* \\ &= -\alpha_1 \text{sgn}(S_1) + \frac{\Delta lx_1}{l} + \frac{\Delta rx_1}{l} - \frac{\omega \Delta lx_1}{l} + \frac{\Delta E_d}{l} + \frac{\phi_d}{l} - \dot{x}_1^* \\ &= -\alpha_1 \text{sgn}(S_1) - \frac{\xi_d}{l} + \dot{x}_1^* \\ &= -\alpha_1 \text{sgn}(S_1) + \eta_{d1} \end{aligned}$$

Since  $|\eta_d| < \alpha_1$ ;  $S_1 \dot{S}_1 \leq 0$  and the surface  $S_1 = 0$ , it is finite time reachable. The dynamics of  $S_2$  becoming,

$$\begin{aligned}
\dot{S}_2 &= -\frac{r}{l}x_2 - \omega x_1 - \frac{E_q}{l} + \frac{1}{l}(\Delta r x_2 + \omega \Delta l x_1 + \Delta E_q \dot{x}_2 + \phi_q) + \frac{u_q}{l} \\
\dot{S}_2 &= -\frac{r}{l}x_2 - \omega x_1 - \frac{E_q}{l} + \frac{1}{l}(\Delta r x_2 + \omega \Delta l x_1 + \Delta E_q \dot{x}_2 + \phi_q) + \frac{u_q}{l} \\
&= -\frac{r}{l}x_2 - \omega x_1 - \frac{E_q}{l} + \frac{1}{l}(\Delta r x_2 + \omega \Delta l x_1 + \Delta E_q \dot{x}_2 + \phi_q) \\
&\quad + \frac{1}{l}[-l\alpha_2 \text{sgn}(S_2) + r x_2 + \omega l x_1 + E_q] \\
&= -\frac{r}{l}x_2 - \omega x_1 - \frac{E_q}{l} - \alpha_2 \text{sgn}(S_2) + \frac{r}{l}x_2 + \omega x_1 + \frac{E_q}{l} \\
&\quad + \frac{1}{l}(\Delta r x_2 + \omega \Delta l x_1 + \Delta E_q \dot{x}_2 + \phi_q) \\
&= -\alpha_2 \text{sgn}(S_2) + \frac{\xi_q}{l} \\
&= -\alpha_2 \text{sgn}(S_2) + \eta_q
\end{aligned} \tag{11}$$

Since  $\alpha_2 > 0$  and the surface  $S_2 = 0$ , it is finite time reachable.

### 3.2 Controller II

**Lemma 3.2.** Single-stage three-phase grid-connected PV system represented in the Eqs. (1) and (2) ensures unity power factor and maximum power extraction on the sliding manifold  $M \cong S_1 = S_2 = 0$ .

$$\begin{aligned}
S_1 &= -kx_3^2 C + CKx_3 x_{3ref} - E_d x_1 - E_q x_2 - x_3 \xi_{x_{3ref}} \\
&\quad - Cx_3 \dot{x}_{3ref} \\
\text{where } \xi_{x_{3ref}} &= \frac{1}{x_3}(E_d \Delta x_1 + \Delta E_d(x_1 + \Delta x_1) + E_q \Delta x_2 \\
&\quad + \Delta E_q(x_2 + \Delta x_2)) + \Delta C \dot{x}_3 + \Delta x_3 + i_{pv} + \phi_v \\
S_2 &= x_2, \quad K > 0
\end{aligned} \tag{12}$$

**Proof:** On the manifold  $M = 0$ , i.e.,  $S_1 = S_2 = 0$

$$\begin{aligned}
S_1 &= -CKx_3^2 + CKx_3 x_{3ref} - E_d x_1 - E_q x_2 + \frac{x_3 i_{pv}}{C} + E_d \Delta x_1 + \Delta E_d x_1 + \Delta E_d \Delta x_1 \\
&\quad + E_q \Delta x_2 + \Delta E_q x_2 + \Delta x_2 + \Delta C x_3 \dot{x}_3 + \Delta x_3 x_3 + \xi_{x_3} - Cx_3 \dot{x}_{3ref} = 0
\end{aligned} \tag{13}$$

$$\begin{aligned}
E_d \Delta x_1 + \Delta E_d x_1 + \Delta E_d \Delta x_1 + E_q \Delta x_2 + \Delta E_q x_2 + \Delta x_2 + \Delta C x_3 \dot{x}_3 \\
+ \Delta x_3 x_3 + \frac{x_3 i_{pv}}{C} + \xi_{x_3} - CKx_3^2 + CKx_3 x_{3ref} - Cx_3 \dot{x}_{3ref} = E_d x_1 + E_q x_2
\end{aligned} \tag{14}$$

$$\begin{aligned}
\frac{1}{Cx_3} E_d \Delta x_1 + \frac{1}{Cx_3} \Delta E_d x_1 + \frac{1}{Cx_3} \Delta E_d \Delta x_1 + \frac{1}{Cx_3} E_q \Delta x_2 + \frac{1}{Cx_3} \Delta E_q x_2 + \frac{1}{Cx_3} \Delta x_2 + \frac{1}{C} \Delta C \dot{x}_3 \\
+ \frac{1}{C} \delta x_3 + \frac{1}{C} i_{pv} + \frac{1}{C} \phi_v - K(x_3 - x_{3ref}) - \dot{x}_{3ref} - \frac{1}{Cx_3}(E_d x_1 + E_q x_2) - \dot{x}_{3ref} = \left(\frac{E_d x_1 + E_q x_2}{cx_3}\right)
\end{aligned} \tag{15}$$

$$\begin{aligned}
\frac{1}{C} \left( \frac{1}{x_3} (E_d \Delta x_1 + \Delta E_d(x_1 + \Delta x_2) + E_q \Delta x_2 + \Delta E_q(x_2 + \Delta x_2)) + \Delta C \dot{x}_3 \right. \\
\left. + \Delta x_3 + i_{pv} + \phi_v \right) - \left( \frac{E_d x_1 + E_q x_2}{cx_3} \right) - \dot{x}_{3ref} = K(x_3 - x_{3ref})
\end{aligned} \tag{16}$$

$$Cx_3 \left[ \frac{1}{Cx_3} E_d \Delta x_1 + \frac{1}{Cx_3} \Delta E_d x_1 + \frac{1}{Cx_3} \Delta E_d \Delta x_1 + \frac{1}{Cx_3} E_q \Delta x_2 + \frac{1}{Cx_3} \Delta E_q x_2 + \frac{1}{Cx_3} \Delta x_2 \right. \\ \left. + \frac{1}{C} \Delta C \dot{x}_3 + \frac{1}{C} \Delta x_3 + \frac{1}{C} i_{pv} + \frac{1}{C} \zeta_v - Kx_3 + Kx_{3ref} - \dot{x}_{3ref} = E_d x_1 + E_q x_2 \right] \quad (17)$$

$$kx_3^2 C + CKx_3 x_{3ref} - E_d x_1 - E_q x_2 - x_3 \zeta_{x_3} - Cx_3 \dot{x}_{3ref} = 0 \\ \frac{Cx_3 \zeta_{x_{3ref}}}{C} - Cx_3 Kx_3 + CKx_3 x_{3ref} - Cx_3 \dot{x}_{3ref} = E_d x_1 + E_q x_2 \\ Cx_3 \left[ \frac{\zeta_{x_{3ref}}}{C} - Kx_3 + Kx_{3ref} - \dot{x}_{3ref} \right] = E_d x_1 + E_q x_2 \\ \frac{\zeta_{x_{3ref}}}{C} - Kx_3 + Kx_{3ref} - \dot{x}_{3ref} = \frac{E_d x_1 + E_q x_2}{Cx_3} \quad (18) \\ \left[ \frac{\zeta_{x_{3ref}}}{C} - \left( \frac{E_d x_1 + E_q x_2}{Cx_3} \right) \right] - \dot{x}_{3ref} = K(x_3 - x_{3ref}) \\ \dot{x}_3 - \dot{x}_{3ref} = -k(x_3 - x_{3ref}) \\ x_3 \rightarrow x_{3ref} \text{ as } t \rightarrow \infty, K > 0$$

As  $x_{3ref}$  is computed from the MPPT algorithm, maximum power extraction is achieved.  $S_2 = 0$  implies that  $x_2 = 0$  which further implies that the unity power factor is achieved.

**Proposition 3.2.** The sliding manifold M is finite time reachable using the following control law.

$$u_d = 2lKx_1 + \frac{2KlE_q x_2}{E_d} - \frac{l x_1 x_{3ref}}{x_3} - \frac{E_q l x_2 x_{3ref}}{dx_3 E_d} + rx_1 - \omega l x_2 - E_d \\ + E_q \omega l x_1 + \frac{l E_q \alpha_2 \text{sgn}(S_2)}{E_d} - \frac{E_q \omega l x_2}{E_d} + \frac{l \alpha_1 \text{sgn}(S_1)}{E_d} \quad (19) \\ u_q = -l \alpha_2 \text{sgn}(S_2) + \frac{r}{l} x_2 + \omega l x_1 + E_q$$

where,  $\alpha_1 > |\eta_{d2}|$ ,  $\alpha_2 > |\eta_q|$ .

$$\eta_{d2} = \frac{\zeta_{x_{3ref}}^2}{C} - \frac{E_d x_1 \zeta_{x_{3ref}}}{Cx_3} - \frac{E_q x_3 \zeta_{x_{3ref}}}{Cx_3} - 2Kx_3 \zeta_{x_{3ref}} + x_{3ref} \zeta_{x_{3ref}} - \frac{E_d \zeta_d}{l} - \frac{E_q \zeta_q}{l} \\ - Cx_3 \dot{x}_{3ref} - C \dot{x}_3 \dot{x}_{3ref} + KCx_3 \dot{x}_{3ref} \\ \eta_q = \frac{\zeta_q}{l}, \zeta_q = \Delta r x_2 + \omega \Delta l x_1 + \Delta E_q + \Delta l \dot{x}_2 + \varphi_q$$

**Proof:** The dynamics of  $S_1$  becoming,

$$\dot{S}_1 = -\dot{x}_3 \zeta_{x_{3ref}} - Cx_3 \ddot{x}_{3ref} - C \dot{x}_3 \dot{x}_{3ref} - 2KCx_3 \dot{x}_3 + KC \dot{x}_3 x_{3ref} \\ + KCx_3 \dot{x}_{3ref} - E_d \dot{x}_1 - E_q \dot{x}_2 \quad (20)$$

$$= \dot{x}_3 \zeta_{x_{3ref}} - 2KCx_3 \dot{x}_3 + KC \dot{x}_3 x_{3ref} - E_d \dot{x}_1 - E_q \dot{x}_2 - Cx_3 \ddot{x}_{3ref} \\ - C \dot{x}_{3ref} \dot{x}_3 + KCx_3 \dot{x}_{3ref} \\ = \left( \frac{\zeta_{x_{3ref}}}{C} - \left( \frac{E_d x_1 + E_q x_2}{Cx_3} \right) \zeta_{x_{3ref}} \right) - 2KCx_3 \left( \frac{\zeta_{x_{3ref}}}{C} - \left( \frac{E_d x_1 + E_q x_2}{Cx_3} \right) \right) x_{3ref} \\ - E_d \left( -\frac{rx_2}{l} + \omega x_2 - \frac{E_d}{l} + \frac{u_d}{l} + \frac{\zeta_d}{l} \right) - E_q \left( -\frac{rx_2}{l} - \omega x_1 - \frac{E_q}{l} + \frac{u_q}{l} + \frac{\zeta_q}{l} \right) \\ - Cx_3 \ddot{x}_{3ref} - C \dot{x}_{3ref} \dot{x}_3 + KCx_3 \dot{x}_{3ref} \quad (21)$$

$$\begin{aligned} \dot{S}_1 &= \left( \frac{x_3 \zeta_{x_{3ref}} - E_d x_1 - E_q x_2}{Cx_3} \zeta_{x_{3ref}} \right) - 2K C x_3 \left( \frac{x_3 \zeta_{x_{3ref}} - E_d x_1 - E_q x_2}{Cx_3} \right) \\ &+ KC \left( \frac{x_3 \zeta_{x_{3ref}} - E_d x_1 - E_q x_2}{Cx_3} \right) x_{3ref} + \frac{E_d r x_1}{l} - E_d \omega x_2 + \frac{E_d^2}{l} - \frac{E_d u_d}{l} \\ &- \frac{E_d \zeta_d}{l} + \frac{E_q r x_2}{l} + E_q \omega x_1 + \frac{E_q^2}{l} - \frac{E_q u_q}{l} - \frac{E_q \zeta_q}{l} \\ &- C x_3 \ddot{x}_{3ref} - C \dot{x}_3 \dot{x}_{3ref} + KC x_3 \dot{x}_{3ref} \end{aligned} \quad (22)$$

$$\begin{aligned} &= \frac{\zeta_{x_{3ref}}^2}{C} - \frac{E_d x_1 \zeta_{x_{3ref}}}{Cx_3} - \frac{E_q x_2 \zeta_{x_{3ref}}}{Cx_3} - 2K x_3 \zeta_{x_{3ref}} + 2KE_d x_1 + 2KE_q x_2 \\ &+ x_{3ref} \zeta_{x_{3ref}} - \frac{E_d x_1 x_{3ref}}{x_3} - \frac{E_q x_2 x_{3ref}}{x_3} + \frac{E_d r x_1}{l} - E_d \omega x_2 + \frac{E_d^2}{l} \\ &- \frac{E_d}{l} \left( 2l K x_1 + \frac{2KE_q l x_2}{E_d} - \frac{l x_1 x_{3ref}}{x_3} - \frac{E_q l x_2 x_{3ref}}{x_3 E_d} + r x_1 - \omega l x_2 + E_d \right. \\ &+ \left. \frac{E_q \omega l x_1}{E_d} + \frac{l E_q \alpha_2 \operatorname{sgn}(S_2)}{E_d} - \frac{E_q \omega l x_2}{E_d} + \frac{l \alpha_1 \operatorname{sgn}(S_1)}{E_d} \right) + \frac{E_q r x_2}{l} - \frac{E_d \zeta_d}{l} \\ &+ E_q \omega x_1 + \frac{E_q^2}{l} - \frac{E_q}{l} (-l \alpha_2 \operatorname{sgn}(S_2) + r x_2 + \omega l x_2 + E_q) \\ &- \frac{E_q \zeta_q}{l} - C x_3 \ddot{x}_{3ref} - C \dot{x}_3 \dot{x}_{3ref} + KC x_3 \dot{x}_{3ref} \end{aligned} \quad (23)$$

$$\begin{aligned} &= \frac{\zeta_{x_{3ref}}^2}{C} - \frac{E_d x_1 \zeta_{x_{3ref}}}{Cx_3} - \frac{E_q x_2 \zeta_{x_{3ref}}}{Cx_3} - 2K x_3 \zeta_{x_{3ref}} + 2KE_d x_1 + 2KE_q x_2 \\ &+ x_{3ref} \zeta_{x_{3ref}} - \frac{E_d x_1 x_{3ref}}{x_3} - \frac{E_q x_2 x_{3ref}}{x_3} + \frac{E_d r x_1}{l} - E_d \omega x_2 + \frac{E_d^2}{l} \\ &- \frac{2l K x_1 E_d}{l} - \frac{2K l x_2 E_d E_q}{l E_d} + \frac{l x_1 x_{3ref} E_d}{l x_3} + \frac{l E_d E_q x_2 x_{3ref}}{E_d x_3} - \frac{r x_1 E_d}{l} + \frac{\omega l x_2 E_d}{l} \\ &- \frac{E_d^2}{l} - \frac{\omega l x_1 E_d E_q}{l E_d} - \frac{l E_d E_q \alpha_2 \operatorname{sgn}(S_2)}{l E_d} + \frac{\omega l x_2 E_d E_q}{l E_d} - \frac{l E_d \alpha_1 \operatorname{sgn}(S_1)}{l E_d} + \frac{E_q r x_2}{l} \\ &- \frac{E_d \zeta_d}{l} + E_q \omega x_1 + \frac{E_q^2}{l} + \frac{l E_q \alpha_2 \operatorname{sgn}(S_2)}{l} - \frac{E_q r x_2}{l} - \frac{E_q \omega l x_1}{l} - \frac{E_q^2}{l} - \frac{E_q \zeta_q}{l} \\ &- C x_3 \ddot{x}_{3ref} - C \dot{x}_3 \dot{x}_{3ref} + KC x_3 \dot{x}_{3ref} \end{aligned} \quad (24)$$

$$\begin{aligned} \dot{S}_1 &= -\alpha_1 \operatorname{sgn}(S_1) + \frac{\zeta_{x_{3ref}}^2}{C} - \frac{E_d x_1 \zeta_{x_{3ref}}}{Cx_3} - \frac{E_q x_2 \zeta_{x_{3ref}}}{Cx_3} - 2K x_3 \zeta_{x_{3ref}} \\ &+ x_{3ref} \zeta_{x_{3ref}} - \frac{E_d \zeta_d}{l} - \frac{E_q \zeta_q}{l} - C x_3 \ddot{x}_{3ref} - C \dot{x}_3 \dot{x}_{3ref} + KC x_3 \dot{x}_{3ref} \\ &= -\alpha_1 \operatorname{sgn}(S_1) + \eta_{d2} \end{aligned} \quad (25)$$

Since  $|\eta_{d2}| < \alpha_1$ ;  $S_1 \dot{S}_1 \leq 0$ ;  $K > 0$  and the surface  $S_1 = 0$ , it is finite-time reachable. The dynamics of  $S_2$  becoming,

$$\begin{aligned}
\dot{S}_2 &= -\frac{r}{l}x_2 - \omega x_1 - \frac{E_q}{l} + \frac{1}{l}(\Delta r x_2 + \omega \Delta l x_1 + \Delta E_q \dot{x}_2 + \phi_q) + \frac{u_q}{l} \\
\dot{S}_2 &= -\frac{r}{l}x_2 - \omega x_1 - \frac{E_q}{l} + \frac{1}{l}(\Delta r x_2 + \omega \Delta l x_1 + \Delta E_q \dot{x}_2 + \phi_q) + \frac{u_q}{l} \\
&= -\frac{r}{l}x_2 - \omega x_1 - \frac{E_q}{l} + \frac{1}{l}(\Delta r x_2 + \omega \Delta l x_1 + \Delta E_q \dot{x}_2 + \phi_q) \\
&\quad + \frac{1}{l}[-\alpha_2 \text{sgn}(S_2) + r x_2 + \omega l x_1 + E_q] \\
&= -\frac{r}{l}x_2 - \omega x_1 - \frac{E_q}{l} - \alpha_2 \text{sgn}(S_2) + \frac{r}{l}x_2 + \omega x_1 + \frac{E_q}{l} \\
&\quad + \frac{1}{l}(\Delta r x_2 + \omega \Delta l x_1 + \Delta E_q \dot{x}_2 + \phi_q) \\
&= -\alpha_2 \text{sgn}(S_2) + \frac{\xi_q}{l} \\
&= -\alpha_2 \text{sgn}(S_2) + \eta_q
\end{aligned} \tag{26}$$

Since  $\alpha_2 > 0$  and the surface,  $S_2 = 0$  it is finite-time reachable.

#### 4 Block Diagram Description and Results

A  $3\varphi$  grid-connected photovoltaic system voltages and currents are changed into d-q axis components through the  $abc - dq$  axis formulation shown in Fig. 2. Furthermore,  $d_q$  component control inputs ( $u_d, u_q$ ) are transformed into three-phase voltages and current using  $dq - abc$  axis transformation, which is fed to three-phase inverter switches. The  $q$ -axis current ( $I_q$ ) is set to zero to maintain grid voltage and the current in phase. The photo-voltaic array conveys the output voltage and current, which vary with respect to different values of irradiance and temperature. This controller tracks automatically ( $x_1, x_3$ ) accordingly ( $x_1^*, x_{3ref}$ ) and it makes the essential voltage and current to extract maximum power from the solar array using MPPT techniques, which is transferred to the grid. A state variable  $x_1^*, x_{3ref}$  simultaneously changes with respect to the irradiance and temperature, so that the output current and voltage  $x_1, x_3$  can track the desired extract power of the photovoltaic system. The designed controller's exploration is justified through simulation in the subsequent section.

##### 4.1 Simulation Results and Discussions

This section presents numerical simulations to validate the proposed nonlinear uncertainties controller designs for grid-connected photovoltaic systems using sliding mode. It compares with different surfaces by constant irradiance with constant temperature, variable irradiance with variable temperature, and system parametric uncertainties. The proposed grid-connected PV system is represented in Eq. (3) with the various sliding function Eqs. (8) and (12) in the controller I and II. The parameters of  $R = 2.4 \Omega$ ,  $L = 8.4 \text{ mH}$ ,  $C = 9200 \mu\text{F}$ ,  $\alpha_1 = 10$ ,  $\alpha_2 = 10$  and gain  $k = 5$  are used to design controllers. The simulation result demonstrates capacitor across the dc-link voltage  $x_{3ref}$ ,  $x_1^*$  in the controller I and II tracks absolute with its reference and to the MPPT controller, which shows the potential of MPPT system  $q$ -axis current tends to zero with respect to its mentioned value  $i_{qref} = 0$  this  $d$ -axis current ( $i_d$ ) is determined by PV array output power which has tended to a constant value.

###### 4.1.1 Case I

In this analysis, the laws of the controller I and II Eqs. (10) and (19) are kept at constant irradiance with constant temperature, and the parameters  $R, L, C$  are change 50% of its systems original values shown in Figs. 3a, 3b, 4a and 4b to validate the performance of the controllers I and II through simulation. Due to parametric uncertainty, the controller does not affect the proposed system. Since the sliding manifold ( $S_1$ ) reachable at zero, it shows performance in the Figs. 3e and 4e with maximum power

tracking of photo-voltaic output voltage, current, and power at  $v_{pvdc} = 430.3$  Volt,  $i_d = 7.75$  Amps,  $P = 3334.85$  Watts is verified with Figs. 7g, 7h and 7k.

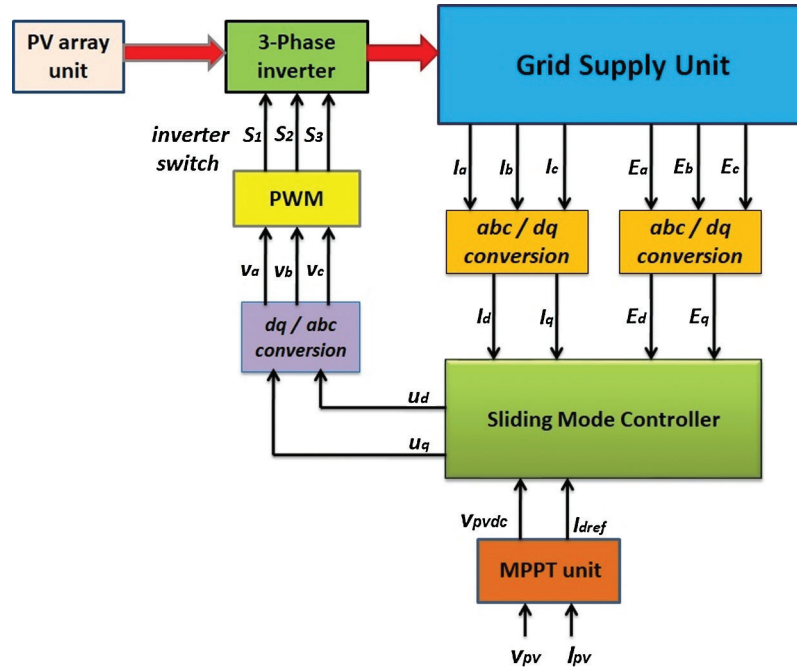


**Figure 2:** Overall proposed controller block diagram

The sliding manifold ( $S_2$ ) reachable at zero, shows the performance of reactive power control operation by the waveforms of grid line current and grid line voltage in the Figs. 3g, 4g, and 3h, 4h revealing synchronized at unity power factor from out-of-phase to an in-phase condition. Controllers always make a single-stage grid-connected photovoltaic system as a unity power factor and are stable. Grid line current, inverter voltage, and reactive current ( $i_q$ ) remain the same under parametric uncertainties operating conditions.

#### 4.1.2 Case II

In this analysis, the laws of the controller I and II Eqs. (10) and (19) are kept at constant irradiance with varying temperature, and the parameters  $R$ ,  $L$ ,  $C$  are change 50% of its systems original values shown in Figs. 5a, 5b, 6a and 6b to validate the performance of the controllers I and II through simulation. Due to parametric uncertainty, the controller does not affect the proposed system. Since the sliding manifold ( $S_1$ ) reachable at zero, it shows performance in the Figs. 5e and 6e with maximum power tracking of photo-voltaic output voltage, current, and power at  $v_{pvdc} = 430.3$  Volt,  $i_d = 7.75$  Amps,  $P = 3334.85$  Watts is verified with the Figs. 7g, 7h and 7k. The sliding manifold ( $S_2$ ) reachable at zero, shows the performance of reactive power control operation by the waveforms of grid line current and grid line voltage in the Figs. 5g, 6g, and 5h, 6h revealing synchronized at unity power factor from out-of-phase to an in-phase condition. Controllers always make a single-stage grid-connected photo-voltaic system as a unity power factor and are stable. Grid line current, inverter voltage, and reactive current ( $i_q$ ) remain the same under parametric uncertainties operating conditions.

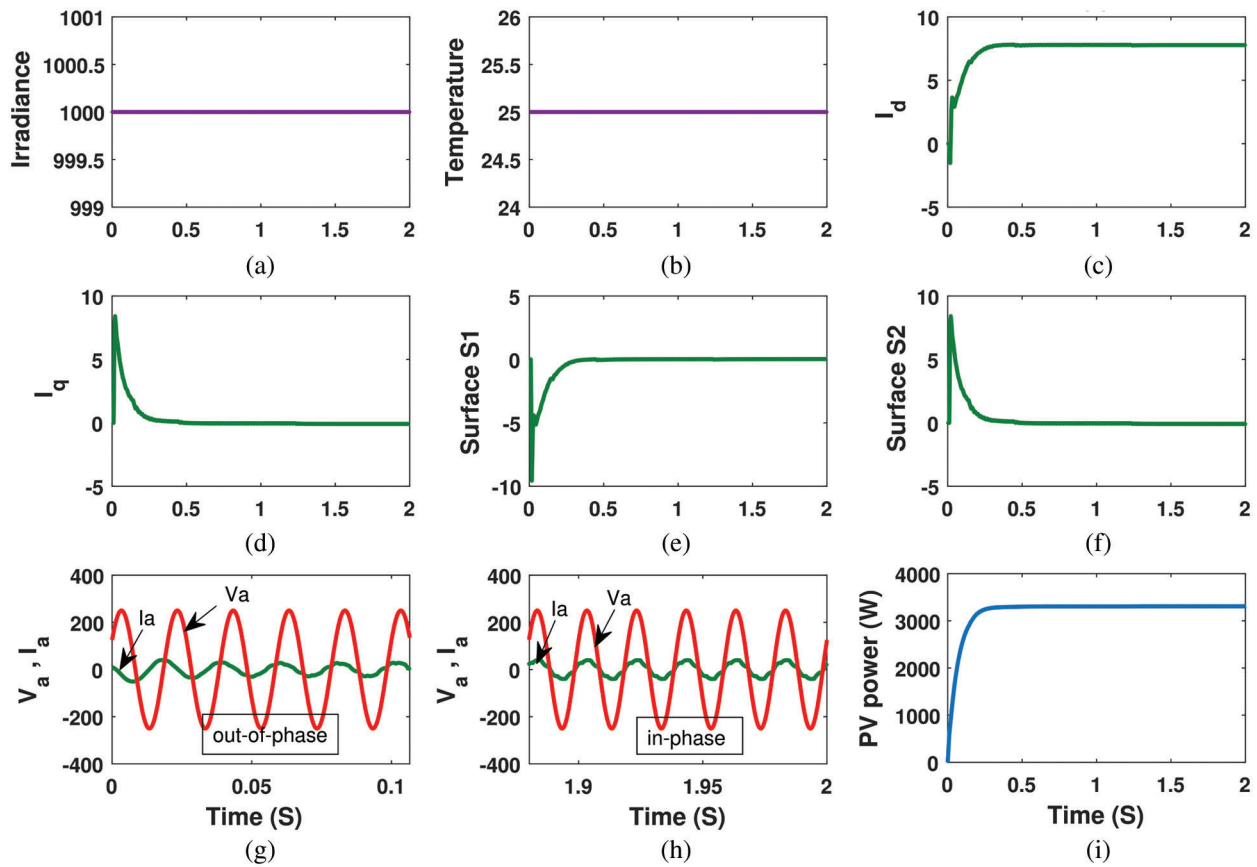


**Figure 3:** Controller I behaviour under standard atmospheric condition

#### 4.1.3 External Unknown Disturbance Robustness Analysis

In this analysis, the laws of the controller I and II Eqs. (10) and (19) are respectively kept at variable irradiance with variable temperature, and their values are changed to 50% of its standard values, as shown in Figs. 7a and 7b, which validates the controller’s performance I and II through simulation. Due to external uncertainty disturbances controller does not affect the proposed system. Since both controllers, I and II sliding manifold ( $S_1$ ) is reachable at zero. It shows the performance in Fig. 7e with maximum power tracking of photo-voltaic output voltage, current, and power at  $P = 3334.85$  Watts,  $v_{pvdc} = 430.3$  Volt,  $i_d = 7.75$  Amps so as to be verified with Figs. 7g, 7h and 7k. Both the controllers I and II sliding manifold ( $S_2$ ) reachable at zero in Fig. 7f, and it shows their performance of reactive power control operation by waveforms of grid line current and grid line voltage while in Figs. 7i and 7j are synchronized at the unity power factor from an out-of-phase to an in-phase condition. Controllers make a single-stage grid-connected photo-voltaic system as a unity power factor and are stable. Since grid line current, inverter voltage, and reactive current ( $i_q$ ) remain the same under external disturbances except sliding manifolds ( $S_1$ ).

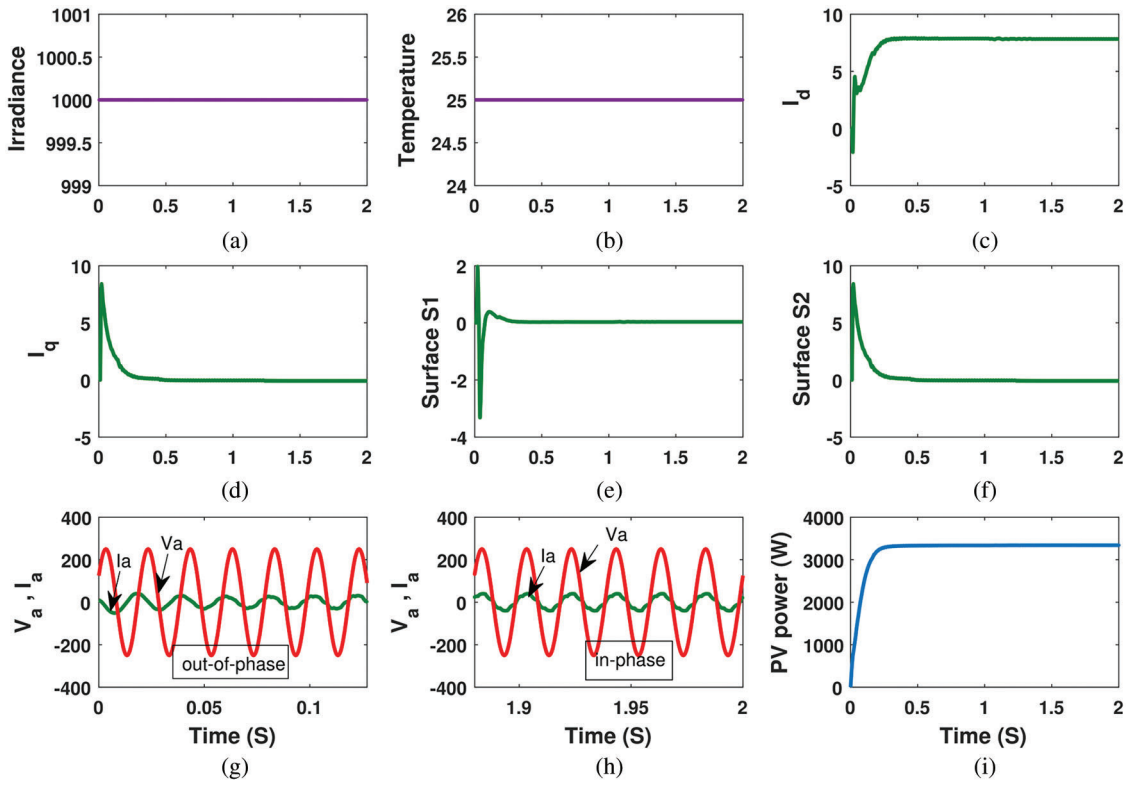


**Figure 4:** Controller II behaviour under standard atmospheric condition

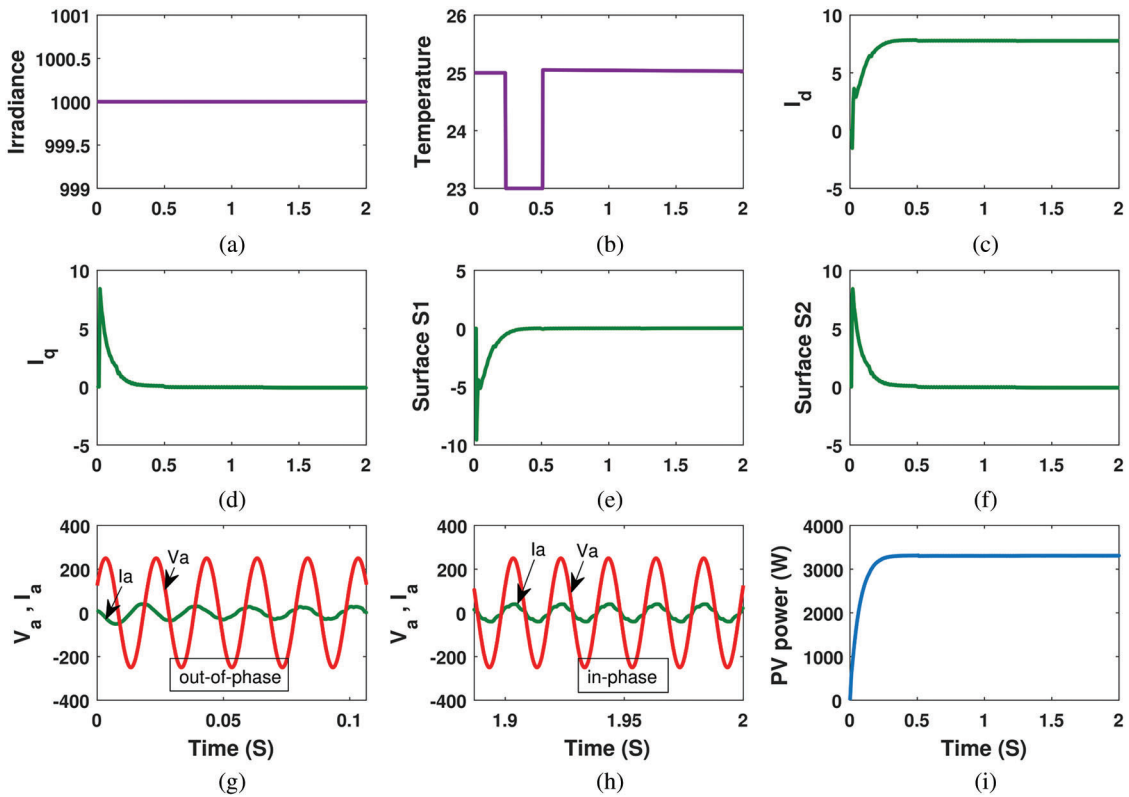


**Figure 5:** Controller I behaviour under constant irradiance and varying temperature condition

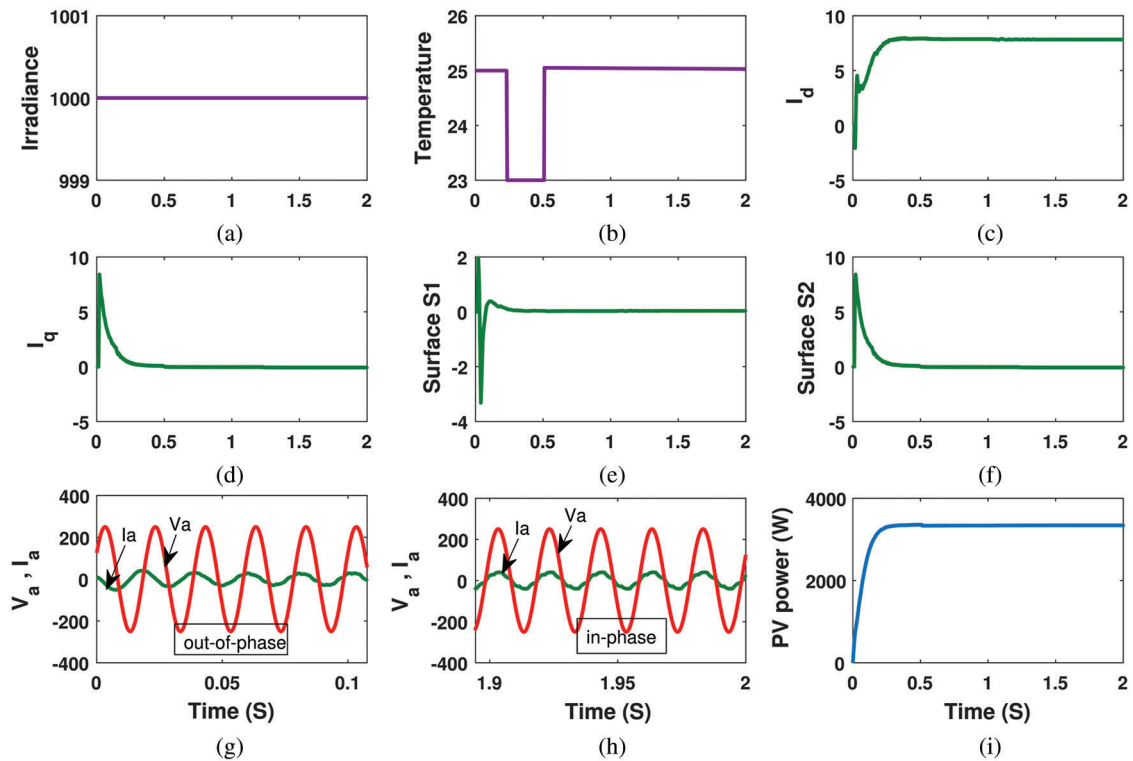


**Figure 6:** Controller II behaviour under constant irradiance and varying temperature condition

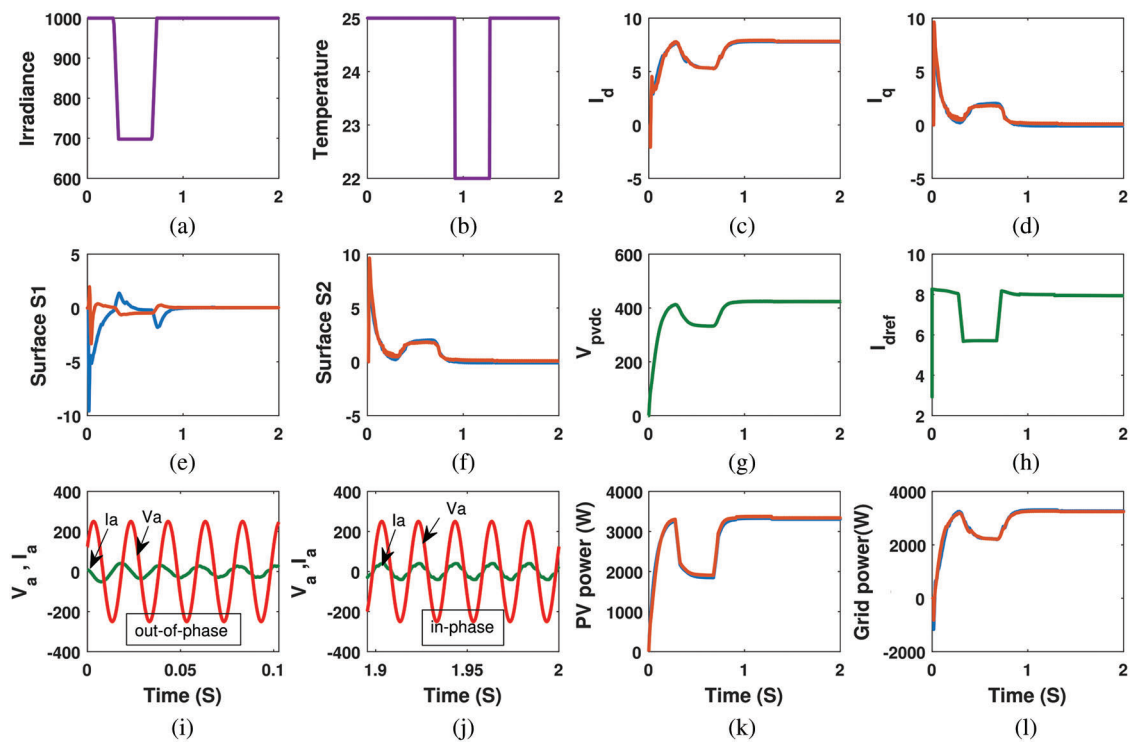


**Figure 7:** Controller I (blue) and II (brown) behaviour under varying atmospheric condition

#### 4.2 Comparison of Controller I and Controller II

Finally, the proposed sliding mode control design compared with different sliding manifolds under different operation conditions such as parametric uncertainty changes in the system and irradiances, temperature disturbances in the solar array input to validate robustness through standard performances. In the proposed system, control techniques, there is no need to change any controller gain values for the occurrence of uncertainties and external disturbances by the proper selection of the sliding manifolds in the control designs to show their robust performance. From the simulation analysis, controller I and II have the only difference in sliding manifold ( $S_1$ ) and reach zero in Fig. 7e. To extract maximum power from the solar array and transfer it to the grid by regulating dc-link voltage across the capacitor in controller II ensures fast and good finite time convergence at the equilibrium point with assured error tracking dynamics compared to a controller I by regulating referenced-axis current. But the controller II, under different operating conditions, does not affect any output of the photo-voltaic system. So the proposed system is stable by controlling  $q$ -axis current ( $i_q = 0$ ) using the dc-link voltage  $v_{pvdC}$  of the proposed system. Also, it is observed that the effect of external variations is less in the performance for nonlinear control design II based on voltage reference sliding surfaces manifolds satisfies with  $M \cong S_1 = S_2 = 0$  condition at finite-time under different disturbances. But controller I, based on current reference sliding surface manifolds, is not satisfied with the  $M \cong S_1 = S_2 = 0$  conditions. However, the difference can be seen from the plot of sliding functions  $S_1$ ,  $S_2$ ,  $d$ -axis current, and control input  $u_1$ . Furthermore, the control input  $u_2$  remains the same for different operating conditions.

#### 5 Conclusion

Two nonlinear sliding mode controllers are designed for a proposed grid-connected PV system to extract and transfer maximum power from a solar array to a grid to ensure the unity power factor. A proposed controller II performances have good robustness versus uncertainty disturbances and parameter variations of the PV systems compared to Controller I. The proposed system controller II is more stable under different operating conditions. A controller II does not limit the parametric uncertainties and disturbances on the system, which shows the significance of the developed designs compared to controller I. The stability of the PV system has proved through numerical simulation for both normal and robust conditions.

**Acknowledgement:** The authors would like to thank the management of the National Institute of Technology, Tiruchirappalli, India, and GMR Institute of Technology, Rajam, India, for providing laboratory facilities to conduct the research.

**Funding Statement:** The author(s) received no specific funding for this study.

**Conflicts of Interest:** The authors declare that they have no conflicts of interest to report regarding the present study.

#### References

1. Tafti, H. D., Maswood, A. I., Konstantinou, G., Pou, J., Blaabjerg, F. (2018). A general constant power generation algorithm for photovoltaic systems. *IEEE Transactions on Power Electronics*, 33(5), 4088–4101. DOI 10.1109/TPEL.2017.2724544.
2. Nadia, A. R., Isa, N. A. M., Desa, M. K. M. (2017). Advances in solar photovoltaic tracking systems: A review. *Renewable and Sustainable Energy Reviews*, 82(3), 2548–2569.
3. Anzalchi, A., Sarwat, A. (2017). Overview of technical specifications for grid-connected photovoltaic systems. *Energy Conversion and Management*, 152, 312–327. DOI 10.1016/j.enconman.2017.09.049.
4. Premkumar, M., Vijaya Krishna, R., Mohan Kumar, R., Sowmya, R. (2019). Protection to grid tied converters and power quality control using active shunt filter. *International Journal of Engineering and Advanced Technology*, 8 (3), 449–456. DOI 10.35940/ijeat.E1063.0585C19.

5. Lal, V. N., Singh, S. (2017). Control and performance analysis of a single-stage utility-scale grid-connected PV system. *IEEE Systems Journal*, 11(3), 1601–1611. DOI 10.1109/JSYST.2015.2408055.
6. Wu, T. F., Chang, C. H., Lin, L. C., Kuo, C. L. (2011). Power loss comparison of single-and two-stage grid-connected photovoltaic systems. *IEEE Transactions on Energy Conversion*, 26(2), 707–715. DOI 10.1109/TEC.2011.2123897.
7. Liang, T. J., Kuo, Y. C., Chen, J. F. (2001). Single-stage photovoltaic energy conversion system. *IEE Proceedings-Electric Power Applications*, 148(4), 339–344. DOI 10.1049/ip-epa:20010436.
8. Huerta, H., Loukianov, A., Cañedo, J. (2018). Passivity sliding mode control of large-scale power systems. *IEEE Transactions on Control Systems Technology*, 27(3), 1219–1227. DOI 10.1109/TCST.2018.2791928.
9. Merabet, A., Labib, L., Ghias, A. M., Ghenai, C., Salameh, T. (2017). Robust feedback linearizing control with sliding mode compensation for a grid-connected photovoltaic inverter system under unbalanced grid voltages. *IEEE Journal of Photovoltaics*, 7(3), 828–838. DOI 10.1109/JPHOTOV.2017.2667724.
10. Mahmud, M., Pota, H. R., Hossain, M. J., Roy, N. (2014). Robust partial feedback linearizing stabilization scheme for three-phase grid-connected photovoltaic systems. *IEEE Journal of Photovoltaics*, 4(1), 423–431. DOI 10.1109/JPHOTOV.2013.2281721.
11. Premkumar, M., Umashankar, S., Sudhakar Babu, T., Sanjeevikumar, P., Holm-Nielsen, J. B. et al. (2020). Improved perturb and observation maximum power point tracking technique for solar photovoltaic power generation systems. *IEEE Systems Journal*, 01–12. DOI 10.1109/JSYST.2020.3003255.
12. Kim, I. S. (2006). Sliding mode controller for the single-phase grid-connected photovoltaic system. *Applied Energy*, 83(10), 1101–1115. DOI 10.1016/j.apenergy.2005.11.004.
13. Kim, I. S. (2007). Robust maximum power point tracker using sliding mode controller for the three-phase grid-connected photovoltaic system. *Solar Energy*, 81(3), 405–414. DOI 10.1016/j.solener.2006.04.005.
14. Danandeh, M. S. M., Mousavi, G. (2017). Comparative and comprehensive review of maximum power point tracking methods for PV cells. *Renewable and Sustainable Energy Reviews*, 82(3), 2743–2767. DOI 10.1016/j.rser.2017.10.009.
15. Benamor, A., Chrifi-Alaoui, L., Messaoud, H., Chaabane, M. (2011). Sliding mode control, with integrator, for a class of MIMO nonlinear systems. *Engineering*, 3(5), 435–444. DOI 10.4236/eng.2011.35050.
16. Shang, L., Sun, D., Hu, J. (2011). Sliding-mode-based direct power control of grid-connected voltage-sourced inverters under unbalanced network conditions. *IET Power Electronics*, 4(5), 570–579. DOI 10.1049/iet-pel.2010.0160.
17. Menaga, D., Sankaranarayanan, V. (2020). A novel nonlinear sliding mode controller for a single stage grid-connected photovoltaic system. *ISA Transactions*, 1–11. DOI 10.1016/j.isatra.2020.07.021.
18. Menaga, D., Sankaranarayanan, V. (2020). Performance comparison for grid connected photovoltaic system using sliding mode control. *Journal of King Saud University-Engineering Sciences*, 1–15. DOI 10.1016/j.jksues.2020.04.012.
19. Premkumar, M., Sowmya, R. (2019). An effective maximum power point tracker for partially shaded solar photovoltaic systems. *Energy Reports*, 5, 1445–1462. DOI 10.1016/j.egy.2019.10.006.
20. Subudhi, B., Pradhan, R. (2013). A comparative study on maximum power point tracking techniques for photovoltaic power systems. *IEEE Transactions on Sustainable Energy*, 4(1), 89–98. DOI 10.1109/TSTE.2012.2202294.
21. De Brito, M. A. G., Galotto Jr., L., Sampaio, L. P., de Azevedo e Melo, G., Canesin, C. A. (2013). Evaluation of the main mppt techniques for photovoltaic applications. *IEEE Transactions on Industrial Electronics*, 60(3), 1156–1167. DOI 10.1109/TIE.2012.2198036.
22. Levron, Y., Shmilovitz, D. (2013). Maximum power point tracking employing sliding mode control. *IEEE Transactions on Circuits and Systems I: Regular Papers*, 60(3), 724–732. DOI 10.1109/TCSI.2012.2215760.